International Journal of Fatigue 125 (2019) 199–209

Contents lists available at ScienceDirect

International Journal of Fatigue

journal homepage: www.elsevier.com/locate/ijfatigue

Constraint corrected cycle-by-cycle analysis of crack growth retardation under variable amplitude fatigue loading

Jie Zhang[a,b,*], Louis Muys[b], Steven De Tender[b], Nahuel Micone[b], Stijn Hertelé[b], Wim De Waele[b]

[a] SIM vzw, Technologiepark 48, 9052 Zwijnaarde, Belgium
[b] Soete Laboratory, Department of EEMMeCS, Ghent University, Technologiepark 46, 9052 Zwijnaarde, Belgium

ARTICLE INFO

Keywords:
Fatigue crack growth
Variable amplitude
Retardation
Crack tip plasticity models
Wheeler model

ABSTRACT

Various models exist to predict load interaction effects on fatigue crack growth in variable amplitude loading conditions. Stress overloads have the potential to strongly retard or even arrest a propagating fatigue crack. Whereas global analysis methods (making use of equivalent quantities) allow to describe stochastic loading scenarios, describing the effects of deterministic overloads requires cycle-by-cycle analysis techniques. Within this category, plastic zone models have proven to be effective and pragmatic in terms of calibration. Current models, however, do not account for the effect of crack tip constraint on the plastic zone size, whose estimation is a requirement. This paper develops a novel ("extended") crack growth formulation based on the traditional plastic zone based Wheeler's model, taking into account the effect of out-of-plane constraint (plane stress versus plane strain). Calibration of the model requires characterization of shut-off overload ratios for different stress intensity factor levels. The "extended Wheeler" model gives better agreement with experimental tests results than the original and modified Wheeler model.

1. Introduction

Metal components and structures are often subjected to cyclic loading conditions having a variable amplitude. These conditions are described by theories of "variable amplitude fatigue", which the non-constant nature of cyclic loading is accounted for in the calculation of fatigue lifetime. A good understanding of crack growth is important in damage tolerant design, where the safe operation is achieved by periodic inspection, assessment and potentially repair. Improper accounting for load interaction effects may lead to overly conservative lifetime predictions (e.g. when crack growth retardation is neglected), or unsafe predictions (when the retardation is over-estimated or acceleration is underestimated).

The effects of variable loading on fatigue crack propagation were first observed by the aviation industry [1]. Overloads were observed to decrease the crack growth rate, while underloads led to acceleration of the crack growth rate. The associated investigations were performed on typical aviation materials such as aluminum and titanium alloys, but similar effects have been observed for steels. The primary focus of this study is crack growth retardation due to overload, the effect of which is typically more pronounced than acceleration effects caused by underloads [2–4].

Different approaches have been developed to describe load interaction effects on fatigue lifetime. These can be broadly categorized into global analysis or cycle-by-cycle analysis techniques. In a global analysis the load history is considered in its entirety. A statistical description of the load spectrum leads to a single, equivalent value for stress intensity factor (SIF) (e.g., root mean square value) which can then be inserted into a crack growth law (e.g. Paris-Erdogan equation) to obtain a global crack growth rate. In general, global analysis models may deliver acceptable results if the load sequence is stochastically distributed. However, interaction effects of deterministic load sequences (such as a discrete number of single overloads) cannot be accurately modelled by this approach [5].

With cycle-by-cycle analysis, incremental crack growth is calculated for each load cycle in a prescribed load history. Four analysis types can be identified, notably: models based on crack tip plasticity (e.g., Wheeler [6], Willenborg [7]); models based on crack closure; models based on residual stress calculations in front of the crack tip; predictions based on rigorous finite element modelling of the investigated load sequence. During recent years, several model adaptations were developed to capture overload based retardation effects on fatigue crack growth under variable amplitude loading. Given below is an overview of recent related literature. The evolution of local crack plasticity and its influence on the global elastic stress field was studied by means of the CJP model [8,9], which calculates the size, shape and area of crack

* Corresponding author at: Soete Laboratory, Department of EEMMeCS, Ghent University, Technologiepark 46, 9052 Zwijnaarde, Belgium.
E-mail address: jie.zhang@ugent.be (J. Zhang).

https://doi.org/10.1016/j.ijfatigue.2019.03.046
Received 22 November 2018; Received in revised form 29 March 2019; Accepted 31 March 2019
Available online 01 April 2019
0142-1123/

Nomenclature

a	crack length
a_0	initial crack length
a_n	crack length after n cycles
Δa	crack growth length
a_{OL}	overload crack length
C, m	Paris law constants
n	the number of applied cycles
K	stress intensity factor (SIF)
K_{max},K_{min}	stress intensity factor at maximum and minimum load
K^*_{max}	'no retardation' stress intensity factor
ΔK	stress intensity factor range
ΔK_i	stress intensity factor range of i$^{\mathrm{th}}$ cycle
ΔK_{eff}	effective stress intensity factor range
$\Delta K_{eff,i}$	effective stress intensity factor range for i$^{\mathrm{th}}$ cycle
R	load ratio
R_i	load ratio for i$^{\mathrm{th}}$ cycle
ΔK_{th}	threshold stress intensity factor range
ΔK_{th0}	threshold stress intensity factor range when $R = 0$
ϕ_{wh}	Wheeler's retardation factor
$\phi_{wh,i}$	Wheeler's retardation factor for i$^{\mathrm{th}}$ cycle
ω	shape exponent
r_p	plastic zone size
$r_{p,OL}$	overload plastic zone size
r^*_p	'no retardation' plastic zone size
R_{OL}	overload ratio
R_{SO}	shut-off overload ratio
R_α	correction factor
R'_{SO}	corrected shut-off overload ratio
α	plastic zone size factor
α_{OL}	overload plastic zone size factor
β	exponent in modified Wheeler model
σ_y	yield strength
P	external load
W	specimen thickness
t	specimen thickness
$r_{p,0}$	reference size (plane stress)
τ	normalized thickness
η	global constrain factor
η_{max}, η_{min}	maximum and minimum value of global constrain factor
$r'_{p,0}$	reference size (plane stress) for strip yield model
τ'	normalized thickness for strip yield model

tip plastic zone, leading to modified stress intensity factors to predict residual stress and crack closure. Doing so required cumbersome model calibrations on the basis of measured displacement fields around the crack tip. A unified model based damage mechanics was proposed and validated under different conditions with overload and underload [10], damage accumulation was incorporated with the cyclic plasticity model [11] which describes cyclic strain ratcheting and stress relaxation. Determination of more than 10 material constants for the model makes the model highly complex and challenging to calibrate. Two extra multiplication factors were added to the original Wheeler model retardation factor to catch the effects of delayed retardation and overload interaction [12,13]. In addition, the shape exponent of the reduction factor was found variable for different overloads, but the authors did not provide further discussion of methods to calculate its value. Plasticity induced crack closure due to a single overload was numerically studied based on FEM [14,15] and an empirical model and analytical model, which considered the residual plastic wake as "plastic wedges" and the mechanism of crack tip blunting resulting in elimination of residual plastic wedges, were proposed. However, notable differences between the models and finite element results were found in the various loads. Virtual crack annealing models [16,17] based on the crack closure concept were proposed, in which the equivalent plastic zone in the unloading process was introduced. The results indicated that the model could not accurately predict constant load cases and the load cases with a longer block overload, whose number of cycles exceeded 10. Li et al [18] applied a strain hardening factor given by Shih [19] to correct the size of the overload affected zone in the Wheeler model. Counter-intuitively, obtained shape exponents of the reduction factor were negative for retardation effect. By adding a correction factor for equivalent SIF range, Huang [20] included underloading scenarios into the Wheeler model, and updated the three-piecewise function of plastic zone factor proposed by Voorwald [21] into a continuous function by using FE analysis and data fitting. It is clear from the above that Wheeler based models are widely implemented to describe the retardation in the fatigue crack growth, and provide ample potential for improvements and modifications.

A common limitation of all abovementioned approaches is the lack of a straightforward correction of plastic zone size for out-of-plane constraint conditions. The theoretical limits to these conditions are known as plane stress (when out-of-plane stress is zero for infinitely thin structures) or plane strain (when out-of-plane strain is zero for infinitely thick structures). Engineering structures are situated between both extremes and, by definition, cannot be characterized as pure plane stress or pure plane strain. Their out-of-plane constraint conditions are intermediated between both limits, the exact value being determined by the thickness of the structure and the extent of loading (stress intensity factor). As out-of-plane constraint conditions are known to affect the plastic zone size originating from a crack tip, an effect on crack growth retardation is expected. To our knowledge, a crack growth retardation model that analytically takes into account such effect is missing. Additionally, the shape exponent was extensively reported as a non-constant value in the literature. The dependence of this exponent on the load level [6,22,23], which may significantly influence the crack growth behavior under complex loading compared with a single overload case, is challenging to quantify and a reasonable approach to describe and calibrate it is missing.

The ambition of this work is to describe the influence of (sequences

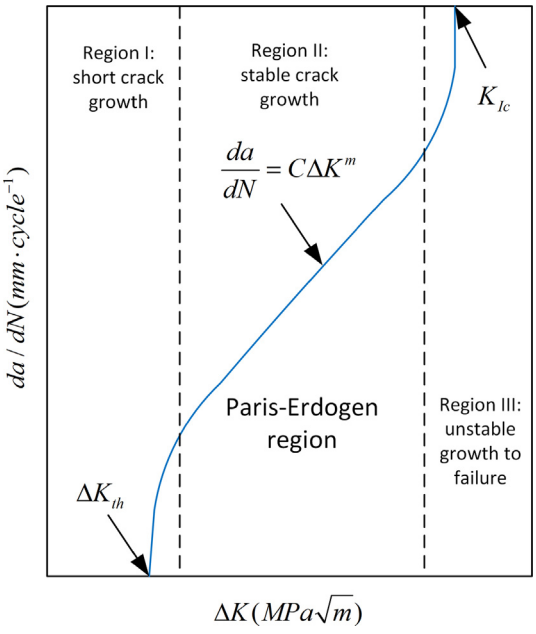

Fig. 1. Typical $da/dN - \Delta K$ relation for fixed R in a logarithmic graph.

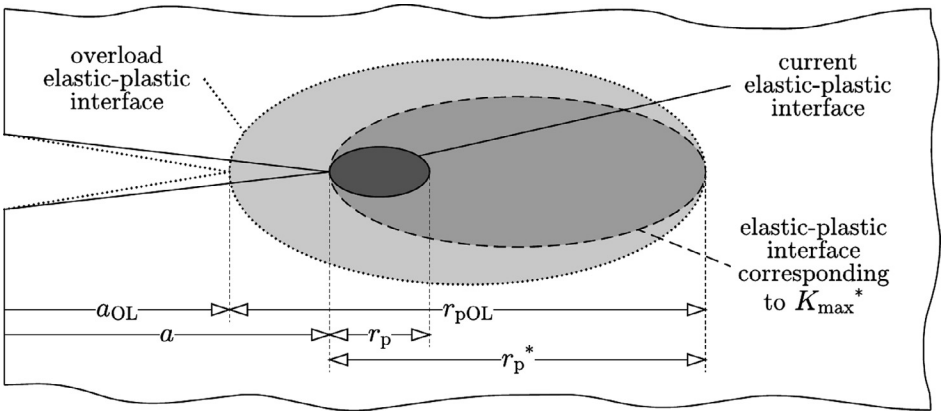

Fig. 2. Post-overload plastic zones considered in crack tip plasticity models.

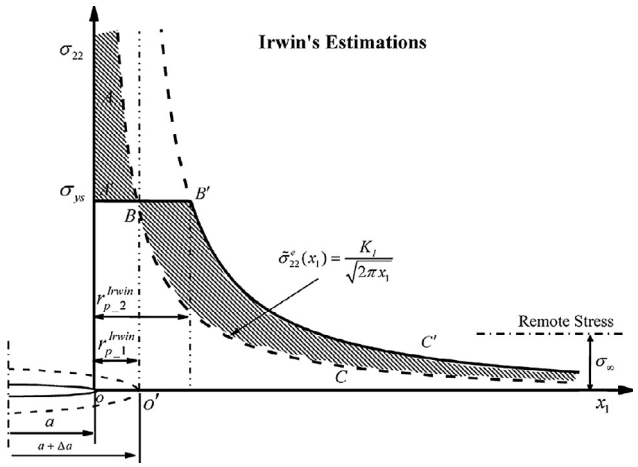

Fig. 3. Irwin's estimation of plastic zone size [31].

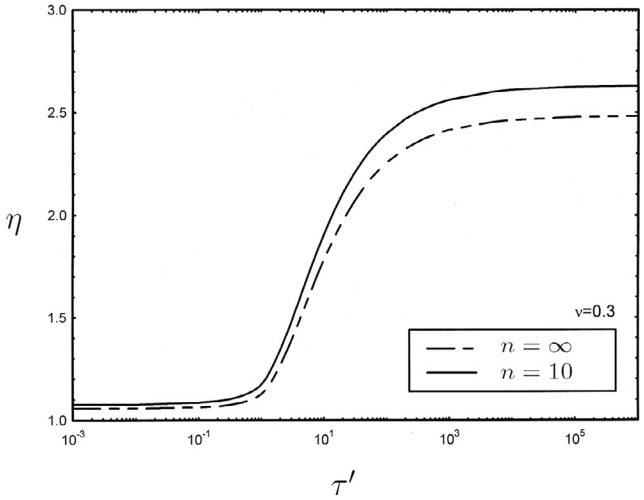

Fig. 5. Influence of τ' and strain hardening on η ().
adopted from [34]

of) overload cycles on the fatigue crack growth in a high strength low alloy steel, making use of cycle-by-cycle analysis and assuming a crack tip plasticity model that accounts for variable out-of-plane constraint conditions. In Section 2, it will be shown that (a) current crack tip plasticity-based models (such as Wheeler's model) do not account for effects of out-of-plane crack tip constraint (e.g., plane stress versus plane strain) on the plastic zone size, and (b) these effects lead to load-dependent shut-off ratios for crack arrest. An "extended Wheeler" model is developed, which does take into account these effects. Section 3 then introduces the numerical framework for cycle-by-cycle crack propagation analysis, in which the extended Wheeler model has been implemented. Sections 4 and 5 compare experimental results with numerically predicted crack growth evolutions, and Section 6 finally concludes.

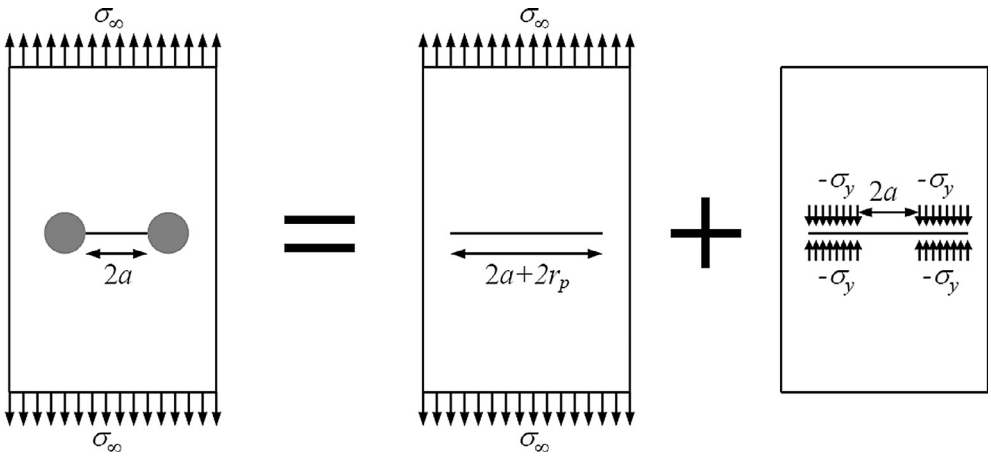

Fig. 4. Visual representation of the strip yield model [33].

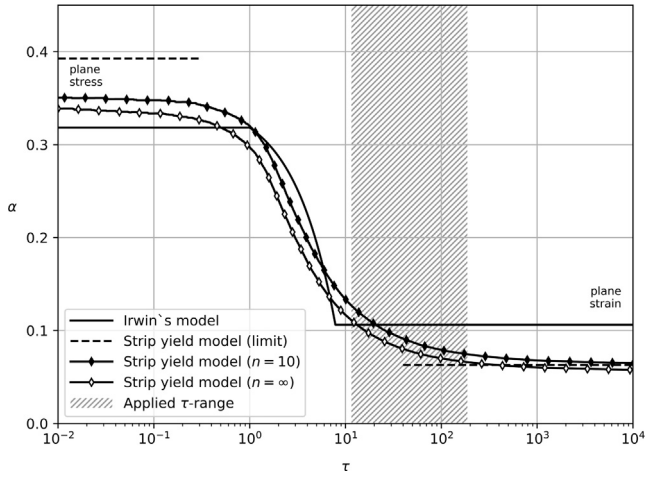

Fig. 6. Comparison of approaches for estimating plastic zone size factor α.

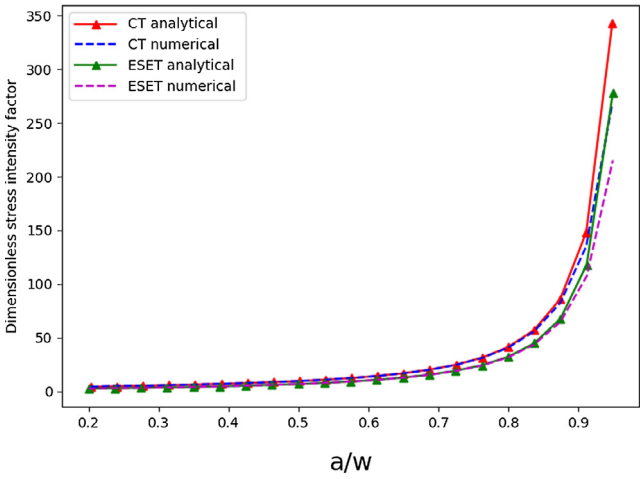

Fig. 8. Comparison between analytical and numerical SIF of ESET and CT specimens.

2. Theoretical background for this study

2.1. Basic fatigue crack growth equations and Wheeler's retardation model

Variable amplitude fatigue crack propagation models generally modify existing crack propagation models for constant amplitude fatigue. Generally, those existing models describe that crack propagation rate is driven by SIF range ΔK and load ratio R, which are functions of K_{max} and K_{min} denoting the SIF at the crack tip at the maximum and minimum load respectively.

$$\frac{da}{dN} = f(\Delta K, R) \tag{1}$$

where $\Delta K = K_{max} - K_{min}$, $R = K_{min}/K_{max}$. As a starting point, the most well-known model proposed by Paris and Erdogan [24], shown in Fig. 1 where C and m are fitted parameters depending on material and loading conditions (e.g., R), describes the second linear stage of typical crack propagation behavior in a double logarithmic graph. Only ΔK is considered in this model, and the influence of different load ratio is not directly included. Furtherly, researchers developed more models taking into account the load ratio effect such Walker's law [25], or to additionally cover the other one or two propagation stages such as

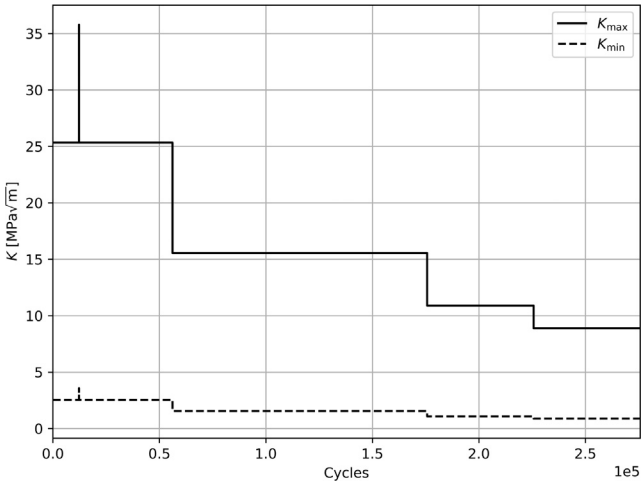

Fig. 9. Load sequence for Wheeler shaping exponent fitting.

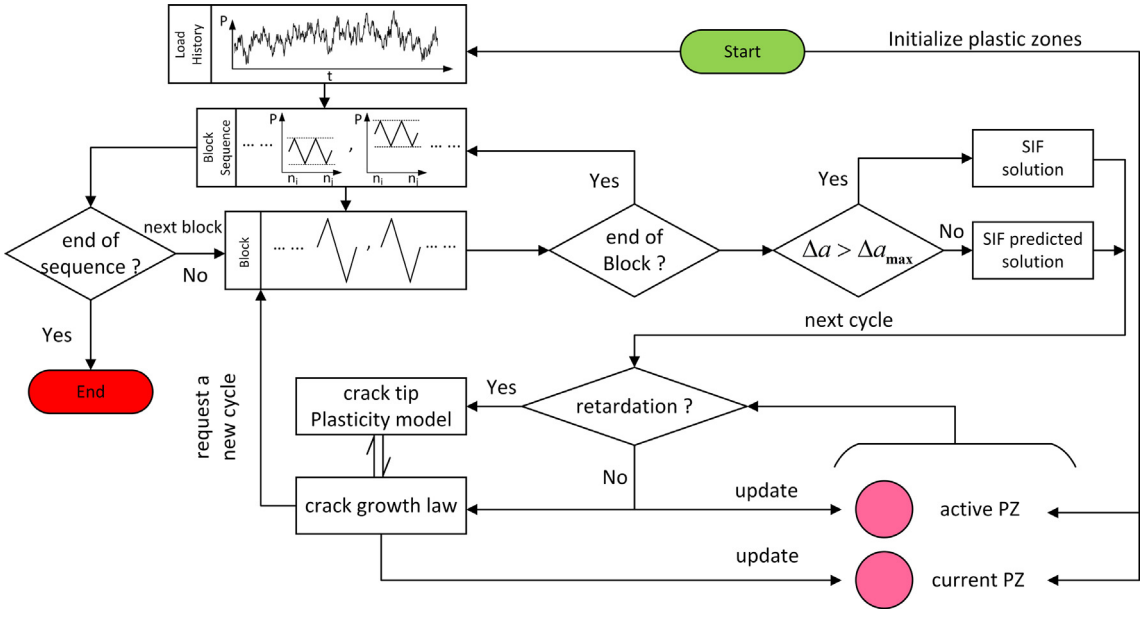

Fig. 7. Overview of crack propagation analysis algorithm.

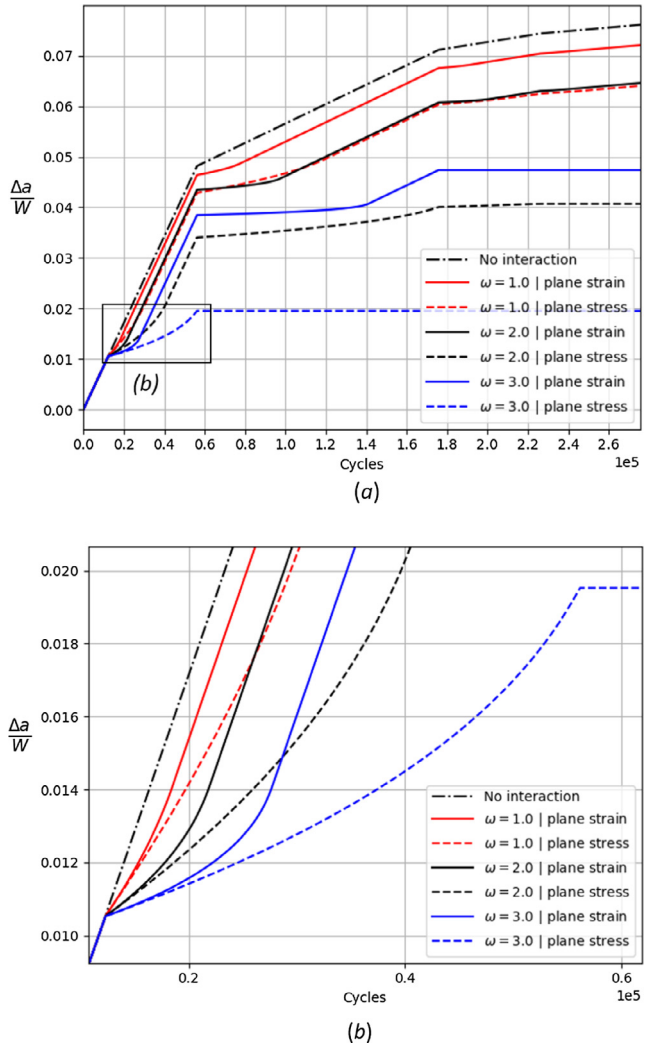

Fig. 10. (a) Influence of plastic zone size factor α and shape exponent ω in the original Wheelermodel; (b) zone in box of retardation effect in different conditions.

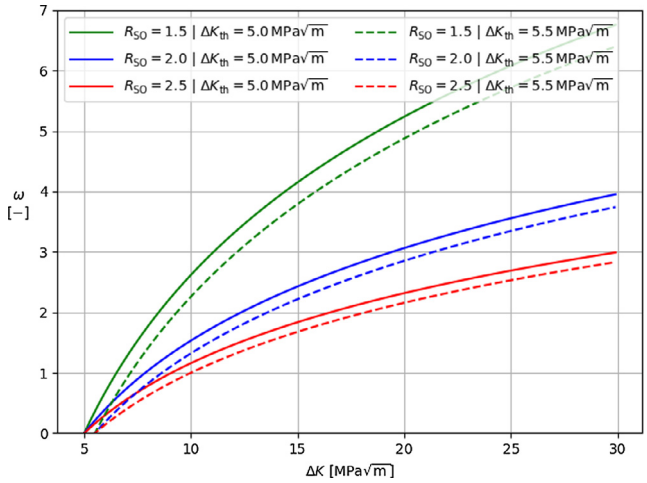

Fig. 11. Influence of shut-off overload ratio R_{SO} and fatigue crack threshold ΔK_{th} on the theoretical shaping exponent.

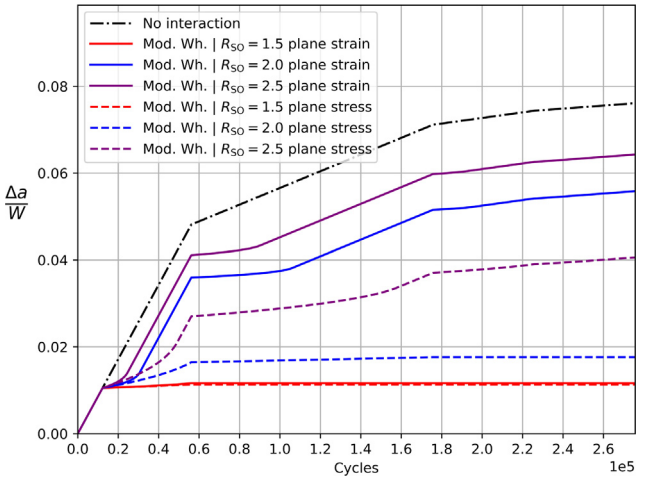

Fig. 12. Influence of shut-off overload ratio R_{SO} in plane stress and plane strain on the modified Wheeler model.

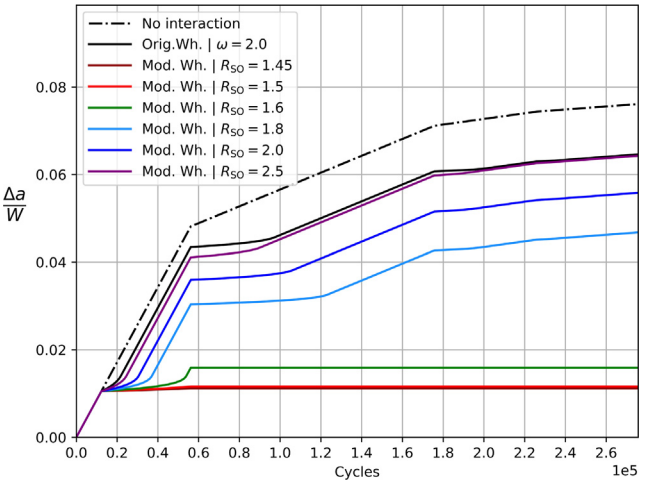

Fig. 13. Influence of shut-off overload ratio R_{SO} in plane strain on the modified Wheeler model.

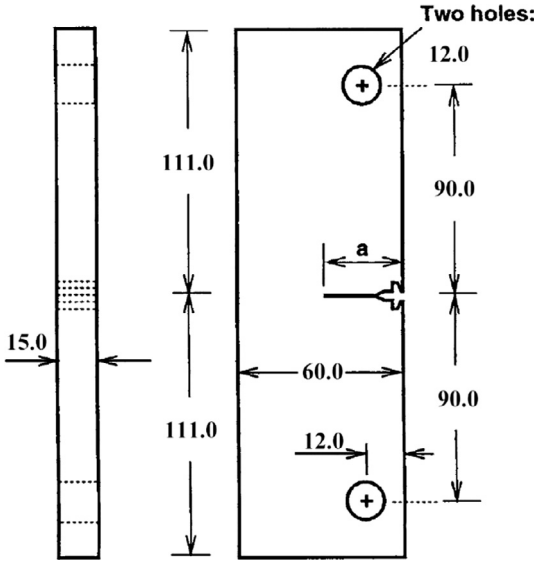

Fig. 14. Configuration of the tested ESET specimens (dimensions in mm).

Table 1
Mechanical properties of DNV F460 steel.

Material	σ_y [MPa]	σ_{UTS} [MPa]	E [GPa]	ν	K_c [MPa·$\sqrt{m}$]	ΔK_{th} [MPa·$\sqrt{m}$]	C [m/cycle]	m
DNV F460	560	635	210	0.28	84.0	5.0	3.6e-12	3.064

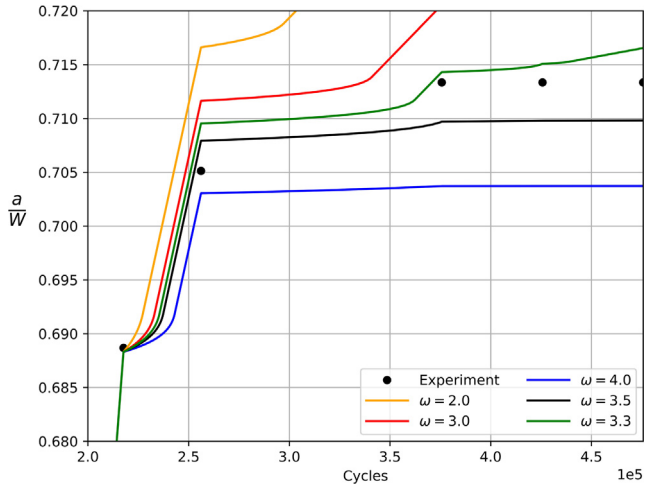

Fig. 15. Wheeler shaping exponent fitting study based on ESET test nr. 1.

Forman's law [26].

Noticing that fatigue lifetime predictions based on linear cumulative crack growth were often found to be ultra-conservative [6], Wheeler modified the non-interaction models for constant amplitude by introducing a retardation factor ϕ_{wh}, which is in the range between 0 and 1, representing the degree of absence of interaction. The Wheeler model does not change input for the crack growth law (e.g. ΔK and R), so the straightforward Paris equation can be employed, provided that its parameters C and m were obtained under the correct load ratio. This is illustrated in Eq. (2), in which n is the number of applied cycles and ΔK_i is the SIF range of cycle i. Load interaction effects can potentially be simulated as the net crack growth rate is no longer independent of prior load history.

$$a_n = a_0 + \sum_{i=1}^{n} \phi_{wh,i} \cdot f(\Delta K_i, R_i) \tag{2}$$

The retardation factor ϕ_{wh} is given in Eqs. (3) and (4). The equations are based on estimations of plastic zone size, which will be further explained in Section 2.2. The state of the material in front of the crack tip considered by crack tip plasticity models is illustrated in Fig. 2. It contains the locations of all relevant elastic-plastic yield interfaces caused by current or previous fatigue cycles and is therefore a representation of relevant loading history. In case of a single overload occurring at crack length a_{OL}, the material yields in the vicinity of the crack tip and a plastic zone of size $r_{p,OL}$ is caused. Subsequent nominal loads, applied at increasing crack length a, will cause plastic zones of size r_p in front of the propagating crack tip. As long as $r_p < r_{p,OL}$, the current plastic zone will be fully embedded in the overload plastic zone for a certain number of cycles due to compressive residual stress. It is assumed that crack growth rate is reduced during these cycles. Once the current elastic-plastic interface intersects the one caused by the overload, the current plastic zone becomes the relevant plastic zone and the interaction effect disappears. Based on this reasoning, the condition for retardation becomes $r_p^* > r_p$ [6]. r_p^* represents the hypothetical size that the current plastic zone should have in order to touch the overload elastic-plastic interface. As the crack propagates, r_p^* will approach r_p, and the retardation effect will weaken till vanish.

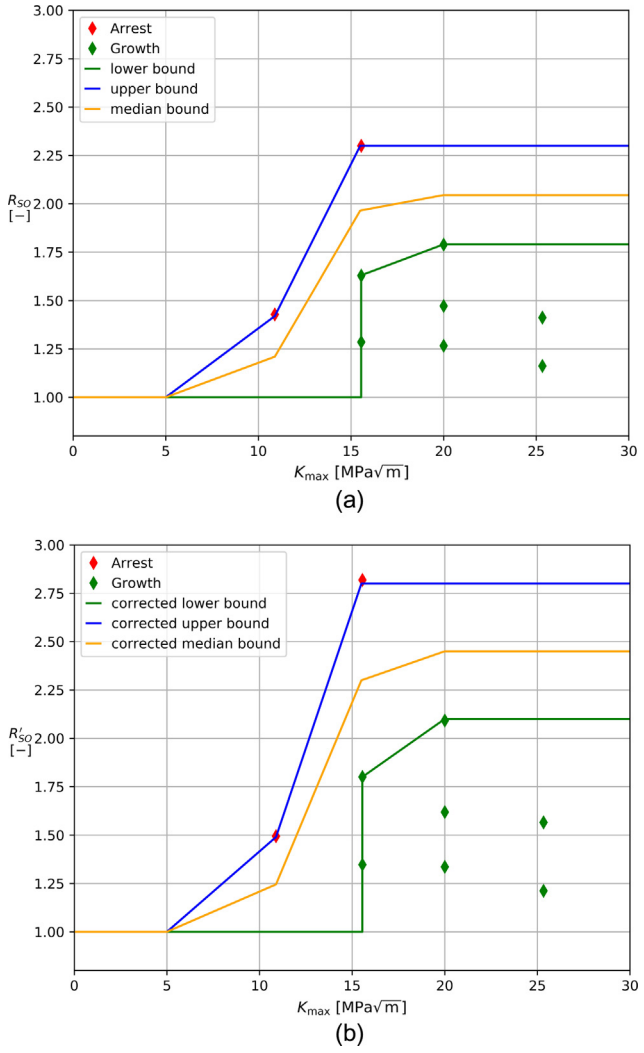

Fig. 16. Estimation of shut-off overload ratio and corrected shut-off ratio of the ESET tested DNV F460 steel.

$$\phi_{wh} = \begin{cases} \left(\frac{r_p}{a_{OL} + r_{p,OL} - a}\right)^{\omega} & a_{OL} + r_{p,OL} > a + r_p \\ 1 & a_{OL} + r_{p,OL} \leqslant a + r_p \end{cases} \tag{3}$$

or

$$\phi_{wh} = \begin{cases} \left(\frac{r_p}{r_p^*}\right)^{\omega} & r_p^* > r_p \\ 1 & r_p^* \leqslant r_p \end{cases} \tag{4}$$

The shape exponent ω is determined experimentally for a given material and type of loading because of dependence on material strength and overload ratio [6,22,23]. Typical reported values range from 1.0 up to 4.0.

As ϕ_{wh} never equals to zero unless K_{max} is zero, the original Wheeler model will never predict crack arrest. However, by introducing ΔK_{eff}, the retardation effect can also be expressed indirectly [27] as Eq. (5)

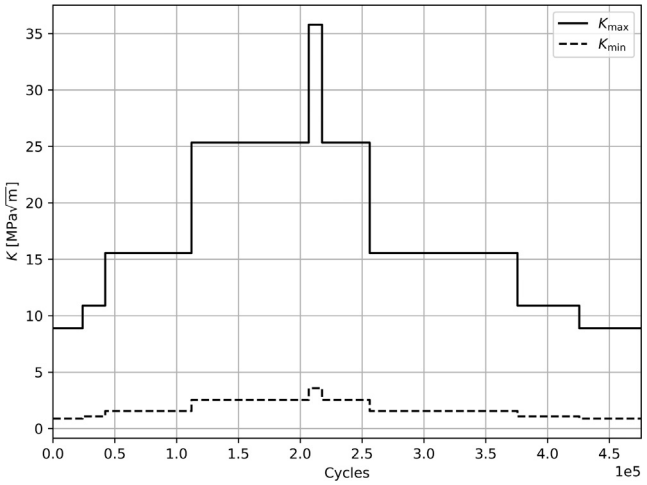

Fig. 17. Simple load scenario: load sequence in LHL test nr. 2.

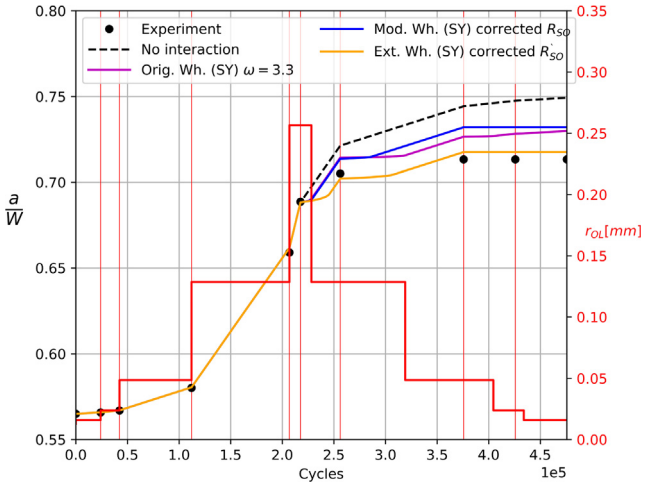

Fig. 18. Simulation results of LHL sequence for ESE(T) specimen in DNV F460 steel test nr. 2.

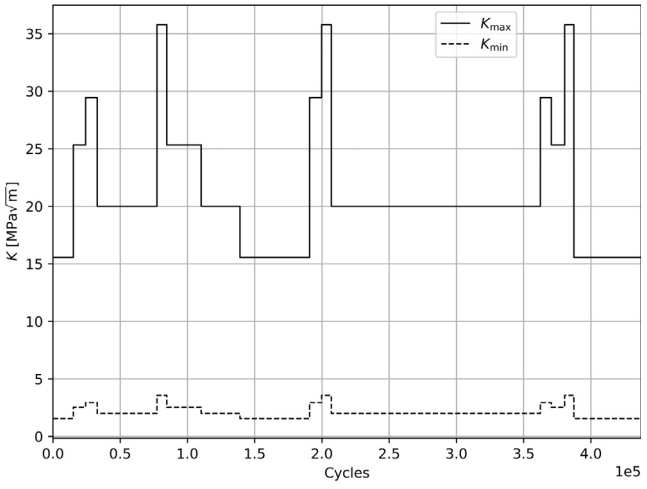

Fig. 19. Complex scenario: semi-random load sequence test nr. 3.

$$a_n = a_0 + \sum_{i=1}^{n} f(\Delta K_{eff,i}, R_i),\ \Delta K_{eff,i} = \phi_{wh,i}^{\beta} \Delta K_i \tag{5}$$

This simple modification can be used with any form of crack growth law which predict both retardation and crack arrest after an overload if $\Delta K_{eff,i} \leqslant \Delta K_{th}$. Its disadvantage is obviously that β is an experimentally fitting value [27]. However, it can be theoretically obtained by Eq. (6) when Paris-Erdogan is applied as a growth rate equation.

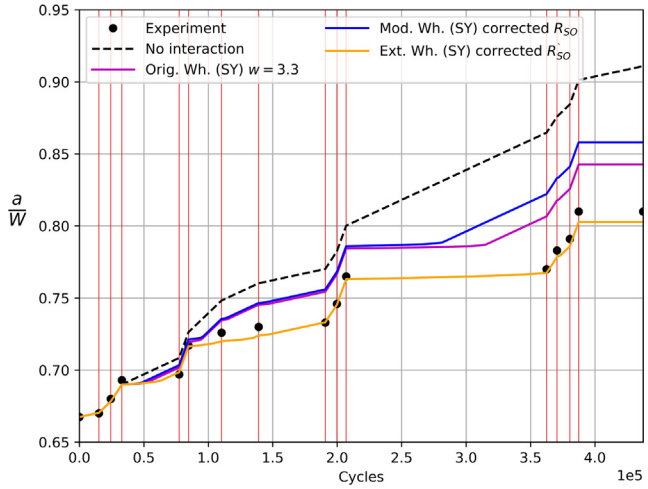

Fig. 20. Simulation results of semi-random sequence for ESE(T) specimen in DNV F460 steel test nr. 3.

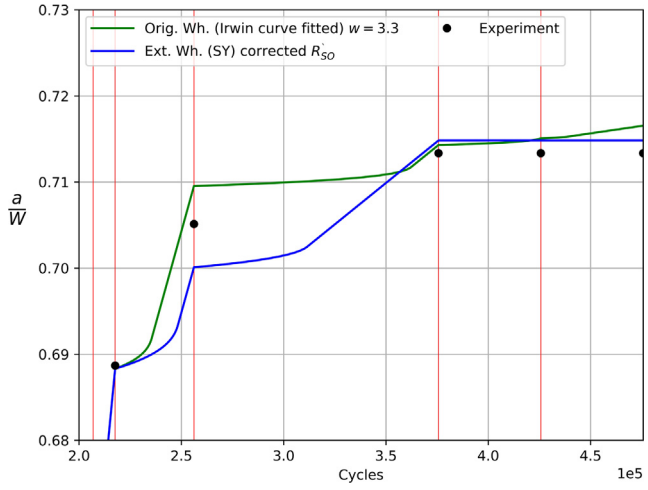

Fig. 21. Prediction of extended model under the first test load compared with curve fitting.

$$a_n = a_0 + \sum_{i=1}^{n} C(R)(\Delta K_{eff,i}),\ \Delta K_{eff,i} = \phi_{wh,i}^{\frac{1}{m}} \Delta K_i \tag{6}$$

Since the model parameters above have not always been experimentally documented and curve-fitting is generally required, a modified Wheeler model based on a theoretical relation was proposed [28,29]. It was based on the observation of crack arrest for overload values exceeding a load ratio value R_{SO} with respect to the nominal load. R_{SO} typically ranges from 1.5 to 3.0, depending on the material. It was reasoned that at the onset of crack arrest, the effective SIF range must not exceed the threshold SIF range for the material. As m is the Paris exponent, the shaping exponent can be determined from readily available material data. It is no longer a constant but a function of the material and the subsequent loading cycles. Assuming a constant α for the time being, in the critical case where the effective SIF ΔK_{eff} equals the threshold ΔK_{th}, the crack arrests to grow and the overload ratio $R_{OL} = R_{SO}$. Then, ω can be obtained by solving the Eq. (7), leading to Eq. (8) (noting that $r_p/r_{p,OL} = R_{SO}^2$ when α is constant, based on Eq. (9) which will be discussed below). For a variable α, the shut-off ratio R_{SO} should be replaced by the more general expression $\sqrt{r_{p,OL}/r_{OL}}$.

$$\Delta K_{th} = (\phi|_{a=a_{OL}})^{1/m} \cdot \Delta K = \left(\frac{r_p}{r_{p,OL}}\right)^{\omega/m} \cdot \Delta K \tag{7}$$

$$\omega = \frac{m}{2}\left(\log\frac{\Delta K_{th}}{\Delta K}/\log\frac{1}{R_{SO}}\right) \tag{8}$$

2.2. Plastic zone size models

Linear elastic stress analysis of sharp cracks predicts infinite stresses at the crack tip, shown in Fig. 3. In reality however, the stresses are finite due to a finite crack tip radius and plastic deformation in front of the crack tip [30]. The general formula for calculating the plastic zone size is given by Eq. (9).

$$r_p = \alpha\left(\frac{K}{\sigma_y}\right)^2 \tag{9}$$

Two main methods for calculating the size of the plastic zone (by means of calibration of α) are proposed in literature [30]: Irwin's model and the strip-yield model.

In Irwin's model, plastic zone size estimation was based, as shown in Fig. 3, on a cut-off of crack tip singularity stresses (line ABC) at the yield strength (line A′B), followed by a shift of the singularity stresses to maintain force equilibrium. Both hatched regions (A′BA and BB′C′C) have an equal area. The resulting stress distribution is line A′B′C′, and the plastic zone size corresponds with line A′B′.

According to Irwin's model, the plastic zone size factor α has a value of $1/\pi(\approx 0.318)$ for plane stress conditions. For plane strain conditions, the value is $1/3\pi(\approx 0.106)$, due to suppression of yielding by the induced triaxial stress state. As neither plane stress nor plane strain are real scenarios, relations have been developed to include the influence of applied load and specimen thickness on the plastic zone size factor α [21]. Considering plastic zone size for plane stress as reference size $r_{p,0}$, a normalized thickness $\tau = t/r_{p,0}$ is introduced. Eq. (10) was proposed to describe the thickness effect in a linear relation between plain stress and plain strain [21,29]. It is emphasized that the plastic zone factor is strongly dependent on load, as it quadratically affects $r_{p,0}$ through K by Eq. (9).

$$\alpha = \begin{cases} \frac{1}{\pi} & \tau < 1 \\ \frac{1}{3\pi} + \frac{2}{3\pi}\cdot\frac{2.5\pi - \tau}{2.5\pi - 1} & 1 \leqslant \tau 2.5\pi \\ \frac{1}{3\pi} & \tau > 2.5\pi \end{cases} \tag{10}$$

The strip yield model was developed by Dugdale and Barenblatt considering small scale yielding conditions as a complement to linear elastic fracture mechanics [32]. The model assumes that all deformation concentrates in a strip in front of the crack. As depicted in Fig. 4, elastic-plastic behavior is approximated by superimposing two elastic solutions for a through crack of length $2a + 2r_p$ in an infinite plate in plane stress. Remote tension over the entire crack length is supplemented with closure stresses at both crack tips over a length r_p the length of the long, slender plastic zone. The closure stress is equal to the yield stress of material. By superposition (expressing that no singularity should occur at the tips of the virtual extended crack having length $2a + 2r_p$), $\alpha = \pi/8$ is calculated [30]. This value is substantially different from the Irwin's approach, and this plane stress plastic zone size $r'_{p,0}$ ($\neq r_{p,0}$) can be used as reference size.

Guo extended the strip model three-dimensionally to obtain valid solutions for plates of finite thickness [34]. A global plastic constrain factor was introduced to include effects of out-of-plane and in-plane constraint to simulate three-dimensional effects in a two-dimensional crack analysis, as shown in Eq. (11):

$$r_p = \frac{\pi}{8}\left(\frac{K}{\eta\sigma_y}\right)^2 \tag{11}$$

For elastic-perfectly plastic materials, $\eta = 1$ in plane stress, and as plate thickness increases, η approaches the plane strain value $\eta_{max} = 1/(1-2\nu)(\approx 2.5)$. Then, the upper bound of α is $\pi/8(\approx 0.393)$, and its lower bound is $\pi(1-2\nu)^2/8(\approx 0.063)$, as denoted in Eq. (12):

$$\alpha\begin{cases} \frac{\pi}{8\eta_{\min}^2} = \frac{\pi}{8} \\ \frac{\pi}{8\eta_{\max}^2} = \frac{\pi(1-2\nu)^2}{8} \end{cases} \tag{12}$$

Between plane stress and plane strain, η is highly dependent on stress levels. A unified curve of η against normalized thickness $\tau' = t/r'_{p,0}$ was obtained, independent of material yield strength, stress level and geometry. For real materials, a minor dependency on the strain hardening exponent n, from the Ramberg-Osgood stress-strain relationship, was observed [35]. Fig. 5 illustrates the influence of τ' and strain hardening on η for an elastic-perfectly plastic material (n being infinite) and a real strain hardening material with $n = 10$. Both were evaluated by finite element analysis [34]. The mathematical description of these curve is based on an iterative procedure described in [34] and not repeated here.

2.3. Development of extended Wheeler model with account for out-of-plane constraint

In the section above, it was already pointed out that the traditional and modified Wheeler's models assume a fixed coefficient $\alpha$for the estimation of plastic zone size. However, Fig. 6 demonstrated a dependency of α on τ, which in turn is influenced by the applied load level. Hence, overload events may have a different plastic zone size coefficient than the follow-up load cycles.

Instead of considering a constant α assumption, a variable α according to load is used for an updated theoretical derivation of ω and R_{SO}. A more general formula for ω is found by a corrected shut-off overload ratio R'_{SO} for the Wheeler model, Eq. (13):

$$R_{SO} = \sqrt{\frac{r_{p,OL}}{r_p}} = \sqrt{\frac{\alpha_{OL}\cdot K_{\max,OL}^2}{\alpha\cdot K_{\max}^2}} = \sqrt{\frac{\alpha_{OL}}{\alpha}}R_{SO} = R_\alpha R_{SO} \tag{13}$$

In other words, a correction factor R_α is introduced to account for the load dependency of α. Shut-off overload ratios R_{SO} are typically measured as a ratio of SIFs when crack arrests, so a transformation to R'_{SO} is needed for an accurate use of the extended Wheeler model. In case a constant value is assumed, $R_\alpha = 1$ and the extended Wheeler model is fully equivalent to the Wheeler model.

3. Cycle-by-cycle crack propagation analysis

As stated above, crack tip plasticity models analyze each applied cycle individually. Therefore, a numerical framework was developed in Python to be able to process a long load history in an automated, cycle-by-cycle way. A schematic overview of this algorithm is given in Fig. 7.

Before the analysis is started, the input load history is translated into a block sequence. It is basically a series of blocks in which every block contains the maximum and minimum applied SIF of the block-specific fatigue cycle and the number of experimentally applied cycles. There are different ways to translate load histories with grouped blocks of sequence, which are likely to produce different retardation effects. Such translations are outside of scope of this paper, here assumes block loading as a starting point of the analysis.

Once the block of load sequence has been defined, the state of the load interaction zone needs to be initialized. The active plastic zone is the largest plastic zone (PZ), possibly caused by an earlier overload cycle, while the current plastic zone is formed by the latest cycle. In the following sections, the cycle-by-cycle analysis framework will be applied to fatigue crack growth rate tests. The input needed for initializing both plastic zones can be derived from the fatigue pre-cracking history of the test specimens. It can be assumed that at the end of this

procedure no load interaction effects were in play, meaning that both plastic zones are equal and can be defined by the initial crack length and the maximum SIF applied during pre-cracking.

After initialization, the first cycle of the first load block is loaded and analyzed. Firstly, the sizes of the current and active plastic zones are compared to decide whether load interaction occurs. After pre-cracking this is not the case, so the active PZ, which is defined as overload elastic-plastic interface with size of $r_{p,OL}$ in Fig. 2, is updated to the current plastic zone. The crack growth law calculates the increment based on the unaltered SIF values and updates the current PZ based on the calculated increment. Further in the load spectrum, an overload can be applied. If the condition for retardation is true, the unmodified SIF values are sent to the crack tip plasticity model, which will alter the input for – or output from – the crack growth law. The modified increment is then used to update the current PZ. Note that the active PZ is not updated since load interaction is occurring.

During the simulation, SIF should be updated cycle-by-cycle based on the load and crack size. This proved straightforward for the laboratory tests reported below, using specimens for which analytical K solutions are available. Differently from analytical solutions for standard geometries, it is impossible for arbitrary geometries to calculate SIF every cycle during the load history because of computational consumption. The framework of Fig. 7 is capable to predict SIF by calculating it intermittently (based on Extended Finite Element Modelling, XFEM) instead of each cycle. Fig. 8 shows examples of comparison between analytical solution and numerical solution of ESET (eccentrically-loaded single edge crack tension) and CT (compact tension) specimens. Hereby, the dimensionless stress intensity factor is defined as Y in Eq. (14). More details are outside the scope of this study, and reported in reference [36].

$$K = \frac{p}{t\sqrt{W}}Y \tag{14}$$

4. Sensitivity analysis of governing parameters

In the crack growth retardation model, many parameters are influential, such as plastic zone size factor α, shaping exponent ω, fatigue crack threshold ΔK_{th} and shut-off overload ratio. A sensitivity study was performed to analyze effects of these parameters based on a tested load profile shown in Fig. 9 (see Section 5 for further detail). All fatigue blocks of loading were applied with $R = 0.1$, starting with a block load having $\Delta K = 22.8\ \text{MPa}\sqrt{\text{m}}$ in order to initiate a stable crack growth. Then, a single overload of $\Delta K = 32.2\ \text{MPa}\sqrt{\text{m}}$ was applied to create an overload plastic zone. Retardation indeed occurred in the following cycles. The load ranges decreased step-wisely in the following load blocks as indicated in the figure.

Various crack growth predictions are shown in Fig. 10. The upper dash-dotted line represents a reference case for which crack growth retardation was neglected (i.e., corresponding with the Paris law). The other lines represent predictions for different crack growth retardation model parameters, adopting the original Wheeler model. The Irwin's model was used to calculated α values for the limit scenarios of plane stress and plane strain.

A first observation is that α has a significant effect on the degree of retardation, as the fatigue crack retards more in plane stress conditions than in plane strain conditions. The explanation is that a higher α (less constrained crack tip) will result in a larger plastic zone. A larger plastic zone size leads to a higher degree of retardation factor and then a lower crack growth rate. It turns out that a correct estimation of plastic zone size is a precondition to achieve accurate crack growth predictions.

Secondly, a strong influence of the shaping exponent ω on crack growth retardation is demonstrated. On the one hand, some effects of α and ω can be separated: α rather affects the duration of retardation, whereas ω rather influences the degree of retardation (initial crack growth slope following an overload). On the other hand, there is a coupled effect: the influence of α (plane stress and plane strain) is more pronounced for higher values of ω.

In Fig. 11, it is clear that ω can vary significantly as a function of load range, so it is not correct to simplify ω as a constant value in the original and modified Wheeler models. The threshold stress intensity factor range is also an influencing parameter, as an increase of ΔK_{th} results in a decrease of ω. Note that ΔK_{th} is relatively sensitive to stress ratio R, according to the following empirical equation [37]:

$$\Delta K_{th} = \Delta K_{th0}(1 - R)^{Y} \tag{15}$$

where ΔK_{th0} represents the fatigue crack growth threshold for $R = 0$; γ is a shaping exponent that varies between 0 and 1, typically 0.5 for mild steels and 0.7–0.9 for pearlitic steels. In practical terms, ΔK_{th} generally does not change much, so its influence will be moderate [38]. The influence of shut-off overload ratio R_{SO} on crack growth predictions is plotted in Figs. 12 and 13. In Fig. 12, similar to what Fig. 11 shows, retardation is quite sensitive to R_{SO} and difference between plane stress and plane strain is even more pronounced. A lower R_{SO} increases ω and the degree of retardation, as the overload ratio R_{OL} is quite close to shut-off. As shown in Fig. 13, when R_{SO} approaches the ratio of the single overload ($R_{OL} = 1.5$), the retardation becomes very close to crack arrest.

5. Comparison with experimental data

This section compares crack growth predictions using different crack tip plasticity-based retardation models against experimental fatigue crack growth rate data, obtained from high strength low alloy steels.

5.1. Material properties and specimen configuration

Different load sequences were applied to 15 mm thick eccentrically-loaded single edge crack tension (ESET) specimens of DNV F460 steel, which is widely used in offshore structures. The configuration of ESET specimens was designed according to the ASTM E647 [39] as shown in Fig. 14. Before testing, specimens were fatigue pre-cracked up to a minimum predefined crack length of about 50% of the specimen width as suggested in the standard. Mechanical properties of DNV F460 steel are listed in Table 1. Particularly, C and m are experimentally obtained Paris-Erdogan parameters.

In Fig. 6, the range of τ values obtained during the ESET tests are shown as a shaded band, along with their corresponding α values according to Irwin's model and strip yield model. τ was in the range between 11.5 and 187.0. The figure indicates that the tests had tendency towards plane strain. Nonetheless, the strip yield model would indicate large variations of α (between 0.063 and 0.393 for perfectly plastic material). These variations would not be captured when using Irwin's plasti zone model, as shown in the same figure. For that reason, the strip yield model will be considered for all further analyses in this paper.

5.2. Experimental evaluation of crack growth retardation models

Three ESET tests were performed with different block load sequences. The rationale behind these sequences is motivated in reference [4] and briefly summarized hereunder. All loading cycles were applied with $R = 0.1$, allowing to use the experimentally calibrated Paris law as a reference, since it was also obtained at this load ratio. The first test comprises a low-high-low sequence with a single cycle overload at peak as shown in Fig. 9, in order to identify necessary material parameters. The second specimen was tested with a low-high-low sequence of block loadings. The third block load sequence was rather random, allowing to check retardation effects in more complex situations. The load sequences are depicted further below in Figs. 17 and 19.

The Wheeler shaping exponent ω is a key parameter to calculate the

retardation effect in the original Wheeler model, ω is calibrated as Wheeler did originally [6] under strip yield modelunder a plane strain plastic zone in the Irwin model. By adjusting the value of ω, the original Wheeler model fitted the experimental data best with $\omega = 3.3$, as shown as green curve in Fig. 15.

Besides the values mentioned above, R_{SO} for the modified Wheeler model and $R_{SO}^{'}$ for the extended Wheeler model were required. It is noticed in Fig. 13 that the sensitivity of crack growth to R_{SO} increases rapidly as it approaches the applied overload ratio R_{OL}. According to the experimental data obtained in different overload cases, all R_{OL} values are plotted as a function of K_{max} (shown upper in Fig. 16); and are distinguished into two groups indicating whether the crack arrests or continues to grow. The assumption of a constant value R_{SO} does not agree with experimental results. In fact, in the range of K_{max} between 5 and 15.5 MPa$\bullet\sqrt{\text{m}}$, an increasing trend of R_{SO} was observed. In order to describe the behaviour of R_{SO}, the available crack arrest and growth data were used as upper and lower bounds to gauge the value. An estimation function for R_{SO} was suggested, shown as the blue curve in Fig. 16. This function will be applied within the modified Wheeler model. Similar to R_{SO}, all $R_{SO}^{'}$ values derived from Eq. (13) are plotted as a function of K_{max} in the bottom part of Fig. 16. An estimation function for $R_{SO}^{'}$ is proposed and will be applied within the modified and extended Wheeler model.

In the following calculations of another two loading cases, the out-of-plane constraint is considered, the strip yield model was applied to obtain the plastic zone size factors in terms of normalized specimen thickness. The average of shut-off ratio and corrected shut-off ratio between upper and lower bound is considered as the load level dependent value for this study.

Firstly, the low-high-low sequence of the second test (shown in Fig. 17) was input. Boundaries between blocks are also indicted by vertical thin red lines in Fig. 18. The strip yield method was used to calculate plastic zone size in the original (with $\omega = 3.3$), modified and extended Wheeler models. he strip yield model was preferred because it yields a more sensible effect of out-of-plane constraint on α in the range of tested conditions, compared to Irwin's plasticity model (recall Fig. 6). In line with our expectations, good correlations are observed in the first five blocks, where no interaction between loads yields, as illustrated in Fig. 18. Following the block with the largest loads, which is the fifth, the retardation effect starts. The black dashed line is the simulation result without any load interaction applied. Both the modified and extended Wheeler models predict the retardation effect better than the analysis without load interaction. Hereby, the extended Wheeler model gives a better agreement than the modified Wheeler model. The original Wheeler model yields the best agreement, This is considered due to the fact that the extended Wheeler model is based on a more accurate description of plastic zone size.

To further evaluate the agreement of different Wheeler model predictions, the semi-random load sequence from Fig. 19 has been input. A mix of overloads were consisted in the scenario. In Fig. 20, the original model gives good correlation, which confirms the validity of Wheeler model again. The experimental agreement of the modified Wheeler model is moderate. In this case, the extended Wheeler model shows the best agreement with experimental data. Since extended Wheeler model has a fully theoretical background while the original one requires the use of a well-tuned empirically ω value, the extended Wheeler model is deemed more convincing.

So far, all extended Wheeler model simulations were based upon the strip yield model. Fig. 21 compares its predictive ability to that of an extended Wheeler model assuming Irwin's plastic zone calculation. Compared with the strip yield model, crack growth predictions deviate more strongly from the experimental data. This is hypothetically due to the observation that the strip yield model provides a more sensible view on out-of-plane constraint effects in Fig. 6.

Looking back to the first test load, prediction of extended model reasonably agrees with the experimental data under the first test load as well (Fig. 21). Hence, the performance of the extended Wheeler model is similar to that of the original Wheeler model in the test that was used to calibrate the latter, and better in two other tests. Based on these observations, it is suggested that the extended Wheeler model provides an improvement to the original model.

6. Conclusions

In this work, the fatigue crack propagation under variable amplitude analysis within a DNV F460 steel was numerically predicted and compared with experimental data. A numerical framework based on cycle-by-cycle plastic zone analysis was established to achieve fatigue crack propagation simulations with a limited computational cost. The baseline for the proposed crack retardation model is the original Wheeler model and a reported modified Wheeler model. The proposed model is based on a more accurate representation of plastic zone size, taking into account effects of out-of- plane constraint (ratio of thickness to plastic zone size). An evolution of shut-off load ratio as a function of stress intensity factor is required to calibrate its parameters, and this evolution can be experimentally obtained. This paper proposes a method to include and calculate the effect of load level on the shape exponent of Wheeler's retardation factor.

The capabilities of the new extended Wheeler model were compared with original and modified Wheeler models, by means of comparison with experimental crack growth data within laboratory tests comprising variable amplitude loading. Combining the extended Wheeler model with the strip yield plastic zone model yields highly accurate representations of the experimental data. It is concluded that the extended Wheeler model offers an opportunity for more accurate fatigue crack growth prediction than the established models, due to its sounder theoretical basis, good predictive abilities and the purely experimental nature of its parameter calibration.

Acknowledgement

The authors gratefully acknowledge the financial support via MaDurOS program (SBO 140151) from Belgian VLAIO (Agency for innovation and business) and SIM (Strategic Initiative Materials in Flanders).

References

[1] Hudson CM, Hardrath HF. Effects of changing stress amplitude on the rate of fatigue-crack propagation in two aluminum alloys. NASA; 1961. Report No.: NASA-TN-D-960, L-1340.
[2] Bacila A, et al. Study of underload effects on the delay induced by an overload in fatigue crack propagation. Int J Fatigue 2007;29(9):1781–7. https://doi.org/10.1016/j.ijfatigue.2007.02.002.
[3] Abdelkader M, et al. Crack propagation under variable amplitude loading. Mat Res 2013;16(5):1161–8. https://doi.org/10.1590/S1516-14392013005000110.
[4] Micone N. Development of testing methodologies for the analysis of variable amplitude fatigue and corrosion-fatigue of offshore steels. Ghent University; 2017.
[5] Sander M. Comparison of fatigue crack growth concepts with respect to interaction effects. In: The 15th European conference on fracture. Stockholm, Sweden; 2004.
[6] Wheeler OE. Spectrum loading and crack growth. J Basic Eng 1972;94(1):181–6. https://doi.org/10.1115/1.3425362.
[7] Willenborg J, Engle RM, Wood HA. A crack growth retardation model using an effective stress concept. Air Force Flight Dynamics Lab; 1971. Report No.: AFFDL-TM-71-1-FBR.
[8] James MN, et al. Local crack plasticity and its influences on the global elastic stress field. Int J Fatigue 2013;46:4–15. https://doi.org/10.1016/j.ijfatigue.2012.04.015.
[9] Vasco-Olmo JM, et al. Crack tip plastic zone evolution during an overload cycle and the contribution of plasticity-induced shielding to crack growth rate changes. Fatigue Fract Eng M 2018;41(10):2172–86. https://doi.org/10.1111/ffe.12840.
[10] Ding Z, et al. An experimental investigation and prediction of fatigue crack growth under overload/underload in Q345R steel. Int J Fatigue 2017;98:155–66. https://doi.org/10.1016/j.ijfatigue.2017.01.024.
[11] Jiang Y, Sehitoglu H. Modeling of cyclic ratchetting plasticity, Part I: Development of constitutive relations. J Appl Mech 1996;63(3):720–5. https://doi.org/10.1115/1.2823355.
[12] Mehrzadi M, Taheri F. A material sensitive modified wheeler model for predicting the retardation in fatigue response of AM60B due to an overload. Int J Fatigue 2013;55:220–9. https://doi.org/10.1016/j.ijfatigue.2013.06.022.

[13] Yuen BKC, Taheri F. Proposed modifications to the Wheeler retardation model for multiple overloading fatigue life prediction. Int J Fatigue 2006;28(12):1803–19. https://doi.org/10.1016/j.ijfatigue.2005.12.007.
[14] Baptista JB, et al. A numerical study of the effect of single overloads on plasticity induced crack closure. Theor Appl Fract Mec 2017;88:51–63. https://doi.org/10.1016/j.tafmec.2016.12.001.
[15] Antunes FV, Castanheira FA, Branco R. A numerical analysis of the mechanisms behind plasticity induced crack closure: application to variable amplitude loadings. Int J Fatigue 2016;89:43–52. https://doi.org/10.1016/j.ijfatigue.2015.12.006.
[16] Zhang W, Liu Y. In situ SEM testing for crack closure investigation and virtual crack annealing model development. Int J Fatigue 2012;43:188–96. https://doi.org/10.1016/j.ijfatigue.2012.04.003.
[17] Jiang S, et al. Comparative study between crack closure model and Willenborg model for fatigue prediction under overload effects. Chinese J Aeronaut 2016;29(6):1618–25. https://doi.org/10.1016/j.cja.2016.10.002.
[18] Li S, et al. Effect of single tensile overload on fatigue crack growth behavior in DP780 dual phase steel. Int J Fatigue 2018;106:49–55. https://doi.org/10.1016/j.ijfatigue.2017.09.018.
[19] Shih C. J-integral estimates for strain hardening materials in antiplane shear using fully plastic solution. Mechanics of crack growth. ASTM Int 1976. https://doi.org/10.1520/STP33936S.
[20] Huang X, Torgeir M, Cui W. An engineering model of fatigue crack growth under variable amplitude loading. Int J Fatigue 2008;30(1):2–10. https://doi.org/10.1016/j.ijfatigue.2007.03.004.
[21] Voorwald HJC, Torres MAS, Pinto Júnior CCE. Modelling of fatigue crack growth following overloads. Int J Fatigue 1991;13(5):423–7. https://doi.org/10.1016/0142-1123(91)90600-4.
[22] Alawi H. Designing reliably for fatigue crack growth under random loading. Eng Fract Mech 1990;37(1):75–85. https://doi.org/10.1016/0013-7944(90)90332-B.
[23] Sheu BC, Song PS, Hwang S. Shaping exponent in wheeler model under a single overload. Eng Fract Mech 1995;51(1):135–43. https://doi.org/10.1016/0013-7944(94)00250-L.
[24] Paris P, Erdogan F. A critical analysis of crack propagation laws. J Basic Eng 1963;85(4):528–33. https://doi.org/10.1115/1.3656900.
[25] Walker K. The effect of stress ratio during crack propagation and fatigue for 2024–T3 and 7075–T6 aluminum. Effects of environment and complex load history on fatigue life. ASTM 1970;462:1–14. https://doi.org/10.1520/STP32032S.
[26] Forman RG, Kearney V, Engle R. Numerical analysis of crack propagation in cyclic-loaded structures. J Basic Eng 1967;89(3):459–63. https://doi.org/10.1115/1.3609637.
[27] Miranda AC, et al. Prediction of Fatigue Life and Crack Path in Complex 2D Structural Components Under Variable Amplitude Loading. Fatigue Testing and Analysis Under Variable Amplitude Loading Conditions, ASTM STP, 2001. 1439. https://doi.org/10.1520/STP1439-EB.
[28] Gray T, Gallagher J. Predicting fatigue crack retardation following a single overload using a modified Wheeler model, Mechanics of crack growth. ASTM Int 1976. https://doi.org/10.1520/STP33955S.
[29] Gray TD. Fatigue crack retardation following a single overload. Air Force Flight Dynamics Lab. Report No.: AFFDL-TM-73-137-FBR; 1973.
[30] Anderson TL. Fracture mechanics: fundamentals and applications. 2nd ed. Taylor & Francis; 1994.
[31] Jia YJ, et al. A better estimation of plastic zone size at the crack tip beyond Irwin's model. J Appl Mech 2013;80(5). https://doi.org/10.1115/1.4023642. p. 051014-051014-6.
[32] Dugdale DS. Yielding of steel sheets containing slits. J Mech Phys Solids 1960;8(2):100–4. https://doi.org/10.1016/0022-5096(60)90013-2.
[33] Hertelé S. Fracture mechanics. Leuven ACCO; 2017.
[34] Guo W. Three-dimensional analyses of plastic constraint for through-thickness cracked bodies. Eng Fract Mech 1999;62(4):383–407. https://doi.org/10.1016/S0013-7944(98)00102-7.
[35] Ramberg W, Osgood WR. Description of stress-strain curves by three parameters. NASA 1943.
[36] Zhang J, et al. Modelling framework for 3D fatigue crack propagation in welds of offshore steel structures. In: International conference on integrity: reliability: failure; 2016. INEGI/FEUP (2016).
[37] Beevers CJ. Fatigue crack growth characteristics at low stress intensities of metals and alloys. Met Sci 1977;11(8–9):362–7. https://doi.org/10.1179/msc.1977.11.8-9.362.
[38] Rushton P, Taheri F, Stredulinsky D. Threshold and variable amplitude crack growth behavior in 350WT steel. In: Proc. 21st Int. Conf. on Pressure Vessels and Piping, ASME-PVP; 2002. https://doi.org/10.1115/PVP2002-1291.
[39] ASTM, E647 Standard test method for measurement of fatigue crack growth rates. In: Annual Book of ASTM Standards, Section Three: Metals Test Methods and Analytical Procedures. 2011. p. 628–70.